NanoImpact 22 (2021) 100313

Contents lists available at ScienceDirect

NanoImpact

journal homepage: www.elsevier.com/locate/nanoimpact

Pulmonary toxicity and gene expression changes after short-term inhalation exposure to surface-modified copper oxide nanoparticles

Ilse Gosens [a,*], Pedro M. Costa [b,c], Magnus Olsson [b], Vicki Stone [d], Anna L. Costa [e], Andrea Brunelli [f], Elena Badetti [f], Alessandro Bonetto [f], Bas G.H. Bokkers [a], Wim H. de Jong [a], Andrew Williams [g], Sabina Halappanavar [g,h], Bengt Fadeel [b], Flemming R. Cassee [a,i]

[a] National Institute for Public Health and the Environment, Bilthoven, the Netherlands
[b] Institute of Environmental Medicine, Karolinska Institutet, Stockholm, Sweden
[c] UCIBIO – Applied molecular Biosciences Unit, Department of Life Sciences, School of Science and Technology, NOVA University of Lisbon, Caparica, Portugal
[d] Heriot-Watt University, School of Life Sciences, Edinburgh, UK
[e] National Research Council, Institute of Science and Technology for Ceramics, Faenza, Italy
[f] Department of Environmental Sciences, Informatics and Statistics, University of Venice Ca' Foscari, Venice, Italy
[g] Environmental and Radiation Health Sciences Directorate, Health Canada, Ottawa, Ontario, Canada
[h] Department of Biology, University of Ottawa, Ottawa, Ontario, Canada
[i] Institute for Risk Assessment Studies, Utrecht University, Utrecht, the Netherlands

ARTICLE INFO

Keywords:
Nanoparticles
Copper oxide
Safe-by-design
Pulmonary toxicity
Transcriptomics

ABSTRACT

Copper oxide nanoparticles (CuO NPs) have previously been shown to cause dose-dependent pulmonary toxicity following inhalation. Here, CuO NPs (10 nm), coated with polyethylenimine (PEI) or ascorbate (ASC) resulting in positively or negatively charged NPs, respectively, were evaluated. Rats were exposed nose-only to similar exposure dose levels of ASC or PEI coated CuO NPs for 5 consecutive days. On day 6 and day 27 post-exposure, pulmonary toxicity markers in bronchoalveolar lavage fluid (BALF), lung histopathology and genome-wide transcriptomic changes in lungs, were assessed. BALF analyses showed a dose-dependent pulmonary inflammation and cell damage, which was supported by the lung histopathological findings of hypertrophy/hyperplasia of bronchiolar and alveolar epithelium, interstitial and alveolar inflammation, and paracortical histiocytosis in mediastinal lymph nodes for both types of CuO NPs. Transcriptomics analysis showed that pathways related to inflammation and cell proliferation were significantly activated. Additionally, we found evidence for the dysregulation of drug metabolism-related genes, especially in rats exposed to ASC-coated CuO NPs. Overall, no differences in the type of toxic effects and potency between the two surface coatings could be established, except with respect to the (regional) dose that initiates bronchiolar and alveolar hypertrophy. This disproves our hypothesis that differences in surface coatings affect the pulmonary toxicity of CuO NPs.

1. Introduction

Copper oxide nanoparticles (CuO NPs) are widely studied due to their considerable toxicity towards human cells and following pulmonary exposure in rodents, which is more severe than would be expected from the dissolved metal alone (Karlsson et al., 2008; Lanone et al., 2009; Wang et al., 2012; Wongrakpanich et al., 2016). For example, $CuCl_2$ (used as an ion control) elicited significantly less cytotoxicity when compared to the CuO NPs in a murine macrophage cell line (Líbalová et al., 2018).

CuO NPs have been commonly used as preservatives and disinfectants with a broad range of applications, from the treatment of wood to paint additives and electronics, which may result in significant occupational hazards resulting from inhalation (Brenner et al., 2016;

Abbreviations: ASC, ascorbate; BALF, bronchoalveolar lavage fluid; BMD, benchmark dose; BMR, benchmark dose response; DEGs, differentially expressed genes; FDR, false discovery rate; DLS, dynamic light scattering; GSD, geometric standard deviation; ICP-MS, inductively coupled plasma mass spectrometry; IPA, Ingenuity Pathway Analysis; MMAD, mass median aerodynamic diameter; MPPD, multiple-path particle dosimetry; MT, metallothionein; NPs, nanoparticles; PEI, polyethylenimine.

* Corresponding author.
E-mail address: ilse.gosens@rivm.nl (I. Gosens).

https://doi.org/10.1016/j.impact.2021.100313
Received 13 November 2020; Received in revised form 13 March 2021; Accepted 18 March 2021
Available online 26 March 2021

Pantano et al., 2018). We and others have described the pulmonary toxicity of airborne CuO NPs including damage to bronchoalveolar epithelial cells accompanied by inflammation (Cho et al., 2010; Gosens et al., 2016; Ilves et al., 2019). Moreover, our recent investigations revealed changes at the level of gene expression that are compatible with aggressive hyperplasia and a potential risk of lung pre-neoplasia, corroborated by the (transient) upregulation of oncoproteins (Costa et al., 2018).

According to the safety by molecular design concept, the NPs surface modification with suitable coatings is a strategy often used to potentially reduce their toxicity (Yan et al., 2019). NP surface coating molecules can play a role in the control of NP reactivity by influencing the direct interaction between the coating molecules and the biological target of by affecting colloidal stability and thereby determining their fate in body. Furthermore, coatings can interact with various toxicants, acting as scavenging or complexing agents of ions or ROS, thereby influencing their bioavailability (Sanità et al., 2020).

Previously, we have prepared and investigated a panel of CuO NPs with different surface modifications using murine RAW264.7 macrophage-like cells as a model. Both ascorbate (ASC) and polyethylenimine (PEI) surface modifications, prepared in a phosphate buffer solution, by colloidal self-assembling, resulted in a more well-dispersed NPs in water with a significant decrease of the average hydrodynamic diameter size in comparison with the uncoated (pristine) material. The negative ζ potential of CuO NPs was enhanced by the negative ASC coating, as derived by the presence of surface surrounding phosphate ions. The PEI-coating yielded a positive ζ potential in water, but not in DMEM (Ortelli et al., 2017, for a detailed description of the NPs in various biological media). We noted that positively charged polyethylenimine (PEI) modified NPs were the most cytotoxic while negatively charged ascorbate (ASC) coated NPs where the least cytotoxic (Líbalová et al., 2018). Furthermore, CuO-ASC yielded a lower degree of superoxide production in cells as compared to pristine CuO NPs.

Understanding the molecular mechanisms of nanoparticle toxicity will inform safer and sustainable nanotechnology approaches . However, as pointed out by Buchman et al. (2019), the “redesign strategies will need to be chosen based on the major mode of toxicity”. Shi et al. (2012) applied mercaptocarboxylic acids with different carbon chain lengths for stabilizing CuO NPs and noted that NPs with longer chain ligands had surfaces that were better protected from oxidation and a corresponding lower ROS generating capacity compared to particles with shorter chain ligands. Sun et al. (2015) addressed the safe-by-design concept with respect to fumed silica and found that titanium and aluminum doping was useful in terms of mitigating the cytotoxicity and pro-inflammatory responses of silica NPs in THP-1 cells. In a subsequent study, the authors synthesized a combinatorial library in which CuO was doped with 1–10% Fe and performed hazard screening of doped *versus* non-doped particles in cell lines and zebrafish embryos (Naatz et al., 2017). The authors could show that the Cu^{+}/Cu^{2+} and Fe^{2+}/Fe^{3+} redox species played a major role in the dissolution process and, hence, in determining the toxicity of the NPs.

In general, positively charged NPs have been suggested to bind to cell surfaces and internalised by cells more efficiently when compared to negatively charged NPs (Zhao et al., 2011). For instance, PEI coating of mesoporous silica NPs enhanced uptake in macrophages (Clemens et al., 2012). Taken together, these findings suggest that surface coating of CuO NPs could serve as a means of achieving safer materials, according to the safe-by-design (SbD) approach, and this led us to hypothesize that CuO-ASC NPs could be less toxic than CuO-PEI NPs. To evaluate this in an *in vivo* model, we exposed rats to different doses of CuO-ASC or CuO-PEI and assessed lung response parameters including BALF analysis, histopathology and genome-wide gene expression changes. We compared the toxic effects of the two surface modified CuO NPs using a previously described short-term inhalation protocol (Gosens et al., 2016).

2. Materials and methods

2.1. Nanomaterials

CuO NPs were obtained from a commercial source (PlasmaChem, GmbH, Berlin, Germany). For details on the characteristics of the pristine CuO NPs, see Gosens et al. (2016). Modified CuO stock suspensions were then prepared as described previously (Ortelli et al., 2017). In short, 10 g/L of Cu (1 wt%) in phosphate buffered saline (PBS) was mixed with 10 wt% of either PEI or ASC (Sigma-Aldrich) with respect to the total amount of copper oxide to obtain surface modified CuO NPs. CuO-PEI and CuO-ASC suspensions were filtered using a centrifugal filter unit (Amicon Ultra-15, 10 kDa, Millipore) to remove unabsorbed capping agent. The obtained samples (wet powder, after the elimination of solvent though ultrafiltration) were dried in the oven at T = 100 °C. After drying, thermogravimetric analysis was carried out to determine the real amount of capping agent. To this end, suspensions were heated at a rate of 10 °C/min up to T = 1000 °C in air flux by thermomicrobalance (STA 449C, Netzsch-Gerätebau GmbH, Selb/Bavaria, Germany). The estimated adsorbed amount of citrate or ascorbate resulted 1,3 and 5,8 wt%, respectively, as referred to the total amount of CuO.

CuO PEI and CuO ASC NP stability characterization was assessed in lung simulant fluids Gamble’s solution and artificial lysosomal fluid (ALF) in a similar fashion as previously described for CuO NPs (Gosens et al., 2016). In short, CuO NP dispersions were prepared in simulant fluids at a concentration of 100 mg/L. Samples were taken after 1 and 24 h at 37 °C and passed through centrifugal filter units. The Cu content was determined by inductively coupled plasma optical emission spectrometry (ICP-OES).

2.2. Animals

Specific pathogen free 6 week old male Wistar rats (RjHan:WI) were obtained from Janvier, France. At arrival, the animals were weighed, randomly allocated and were acclimated for 1–2 weeks before starting the experiment. The study design, including five days of exposure and 22 days of recovery are outlined in Suppl. Fig. S1. Before the start of the exposure, the average weight (±SD) of the rats was 240 ± 20 g with the weight evenly distributed among the exposure groups. Animals were weighed after exposure before dissection and once a week during the recovery period. Food and water were provided *ad libitum*, except during the exposure in nose-only tubes. Experiments were performed at the National Institute for Public Health and the Environment in Bilthoven, Netherlands, in accordance with the Principles of Laboratory Animal Care and with the guidelines approved by the Dutch Ethical Committee in full accordance with European legislation.

2.3. Aerosol generation

CuO-PEI and CuO-ASC aerosols were generated from stock suspensions (10 mg/mL, 1% wt) that were diluted in ultrapure water (to 2 mg/mL, 0.2% wt), using a Schlick compressed air spray-nozzle (Düsen-SchlicK, GmbH, Untersiemau/Coburg Germany). The characteristics of the stock solutions are described in Líbalová et al. (2018). The suspensions were continuously stirred on a magnetic stirrer and metered to the spray-nozzle with an adjustable peristaltic pump. The primary aerosol was diluted with pressurized air, heated, and dried in a mixing chamber and further diluted with moisturized air to a total of 38 L per minute (22 °C, 55%RH) and split equally over the two exposure towers. Particle number counts and size distributions were measured daily during the experimental period using a condensation particle counter CPC 3022A and a scanning mobility particle sizer SMPS model 3936 in combination with the OPS 3330 (all from TSI, St. Paul, MN). The mass concentration was measured with a TEOM series 1400a (Rupprecht & Patashnick, Albany, NY). A time weighted average exposure concentration was

calculated from a continuous aerosol collection on 47 mm Teflon filters using a Mettler MC/ME-5 micro-balance. A time weighted mass median aerodynamic diameter MMAD was determined using an eight-stage (+after filter) cascade impactor MOI Model No. 110 (MSP Corp, Minneapolis, MN). A 1-min sample was taken every half hour. A schematic representation of the aerosol generation in given in Suppl. Fig. S2 and a schematic representation of the MOI sampling to determine the MMAD is provided in Suppl. Fig. S3.

2.4. Aerosol exposure

Animals were exposed nose-only to a single generated exposure concentration of CuO-PEI or CuO-ASC, and to clean air as a control for 5 consecutive days. By placing the animals in the exposure set-up for various durations (7 min, 20 min, 1 h and 3 h), different dose levels of exposure were obtained (Suppl, Table S1). Animals exposed for durations shorter than 3 h to the nanomaterial aerosol, were exposed to clean air for the remainder of the 3-h period. This concentration times time (C x T) protocol follows Gosens et al. (2014), according to OECD Guideline 403. A 3-h concentration equivalent is derived by multiplying the duration of exposure by the exposure concentration (designated as dose C x T) and scaling it to the highest exposure duration of 3 h, see Suppl. Fig. S1 for the dose groups dedicated for toxicological examination (n = 5 per group) and organ burden analysis (n = 4 per group), respectively. The animals autopsied at Day 1 after the 5 days repeated exposure were designated as “main” group and the animals autopsied at Day 27–28 were designated as “recovery” group. Based on our *in vitro* experiments (Líbalová et al., 2018), toxicity was expected to be lower following exposure to CuO-ASC. To increase the chance of finding comparable and complete dose-response curves for both CuO-PEI and CuO-ASC, animals were exposed to a slightly higher concentration of CuO-ASC.

2.5. Lung dissection

Animals were weighed at 1 and 22 days after the final exposure day, and were killed by exsanguinations from the abdominal aorta under anesthesia with a mixture of ketamine (75–100 mg/kg) and xylazine (10 mg/kg) administered intramuscularly. Then, the abdomen and thorax were opened, and blood was withdrawn from the abdominal aorta. A cannula was placed in the trachea and the diaphragm was opened. The left lung was clipped, while the right lung was flushed once using 26.7 mL/kg body weight of saline. The flush consisted of 3 up and down movements in order to collect bronchoalveolar lavage fluid (BALF).

2.6. Bronchoalveolar lavage fluid analyses

Bronchoalveolar lavage fluid (BALF) was obtained as described above. Only BALF data with a recovery >60% of the flushing solution was included in the analysis. The reason for a lower recovery rate was accidental damage to the lung before or during flushing, which occurred only in 1 out of 60 animals. The BALF was centrifuged at 400 ×*g* at 4 °C for 10 min. Lactate dehydrogenase (LDH), alkaline phosphatase (ALP), N-acetylglucosaminidase (NAG), γ-glutamyltransferase (GGT), and total protein content was measured in the supernatant using an auto-analyzer (LX20-Pro, Beckman-Coulter, Woerden, Netherlands) according to the manufacturer’s instructions. The cell pellet was suspended in 1 mL of PBS for total cell counts (Coulter counter). Specimens of 400 cells/glass slide were then produced by cytospin preparation.

2.7. Hematology

Blood samples were collected as described above using an EDTA containing system. Hematological parameters were determined in an Advia 120 Hematology Analyzer (Siemens Health Care, Berlin, Germany). The blood parameters determined were: hemoglobin, packed cell volume, red blood cell count, reticulocytes, total white blood cell count, differential white blood cell count, prothrombin time, thrombocyte count, mean corpuscular volume, mean corpuscular hemoglobin, and mean corpuscular hemoglobin concentration. No exposure related changes in hematology parameters were found (data not shown).

2.8. Organ burden analysis

Organs were weighed and prepared as detailed in Gosens et al. (2016), with modifications. In brief, freeze-dried lung, liver, brain, kidney, spleen and heart were acid digested using a microwave (ETHOS 1600, Milestone) assisted method with the following programme: ramp to 250 W for 1 min, 0 W for 1 min, 250 W for 5 min, 400 W for 3 min, 600 W for 3 min. After heating, the sample solutions were diluted and analysed by inductively coupled plasma mass spectrometry (ICP-MS) equipped with single channel Universal Cell (sp-ICP-MS NexION 350XXD, Perkin Elmer). Potential contamination from the laboratory was controlled by adding at least one procedural blank during each digestion session. The limit of detection (LOD) and the limit of quantification (LOQ) were calculated for each sample set as the average of blanks + 3 standard deviations (SD) and as the average of blanks + 10 SDs, respectively. In order to verify the accuracy and repeatability of the method, 6 aliquots of the standard reference material (SRM) NIST 1577c (bovine liver) were analysed every 10 samples. The average Cu concentration (±SD) detected in the SRM was 277 ± 5 mg/kg^{1}, in agreement with the reference value (267 ± 6 mg/kg^{1}). With respect to the certified value, the recovery of Cu ranged from 90 to 101%. Cu concentrations reported for the different organs correspond to three ICP-MS readings and are expressed on a dry weight basis.

2.9. Histopathology

The weight of organs (left lung, left brain hemisphere, kidneys, liver and spleen) of 5 animals of the main study group and recovery groups (Suppl. Fig. S1) was determined prior to preservation in a neutral aqueous phosphate-buffered 4% solution of formaldehyde (10% solution of formalin). Tissues were embedded in paraffin wax, sectioned at 5 μm and stained with hematoxylin and eosin for histological examination. The left lungs were infused and prepared for histopathological examination (3 levels) as previously described (Gosens et al., 2016). Left lungs were examined for all doses of the main group, clean air control and in the recovery group. Mediastinal lymph nodes and nasal cavities (4 levels) were examined for all doses of the main group, the clean air controls and highest dose of the recovery group. Liver, spleen, kidneys, and brain were examined from all main and recovery animals in clean air controls and at the highest dose of the CuO NPs.

2.10. Microarray analysis

Total RNA was isolated from individual rat lungs (n = 5 per experimental condition) with the AllPrep DNA/RNA Mini kit (Qiagen, Hilden, Germany), following the manufacturer’s instructions. Quantification and primary quality assessment were done with a NanoDrop 2000 spectrophotometer (Thermo Fisher Scientific). The RNA integrity number (RIN) for each RNA sample was then determined with an Agilent 2100 Bioanalyzer (Agilent Technologies, Santa Clara, CA), and RIN values were consistently 7. Labelled cDNAs and cRNAs were synthesized from 200 ng of total RNA *per* lung sample using the Linear Amplification Kit or the Universal Rat Reference RNA (both from Agilent). T7 RNA polymerase-transcribed cRNAs were subsequently labelled with Cyanine-5 while UMRR was labelled with Cyanine-3. An equimolar amount of UMRR cRNAs was mixed with each experimental cRNA and hybridized to SurePrint G3 Rat 8 × 60 K microarrays (Agilent). Microarray slides were washed and scanned using a G250B apparatus, with data being retrieved with the software Feature Extraction 10.7.3 (all from Agilent). Further details can be found in Halappanavar et al. (2015).

2.11. Bioinformatics

Microarray data were analysed using R 3.5.x (Ihaka and Gentleman, 1996). Further details can be found in Halappanavar et al. (2015) and Costa et al. (2018). In brief, following data normalization through locally weighted scatterplot smoothing regression modelling from a randomised block design, the significance of differentially expressed genes (DEGs) was determined by the *Fs* statistic with residual shuffling (Cui et al., 2005). The respective p-values were corrected for false discovery rates (FDR), as described by Benjamini and Hochberg (1995). Fold change ratios (FC) relatively to controls were estimated as least-squared means between replicates. A gene was considered differentially expressed if $|FC| > 2$ (up- or downregulated) and FDR-corrected $p < 0.05$. Downstream analyses, including Venn diagrams, hierarchical clustering, functional annotation and gene ontology and gene enrichment were conducted using packages limma, edgeR, biomaRt and KEGGprofile for R, as described previously (Costa et al., 2018). Pathway analysis with causal networks (Krämer et al., 2014) was performed using the Ingenuity Pathway Analysis (IPA) software (application version 220217, content version 16542223, licensed by Ingenuity Systems, Redwood City, CA). Results were filtered by $p < 0.05$ and activation $|Z|$-score > 2.

2.12. ELISA

Lung tissue (100 mg) from each of three rats per clean air control and the highest exposure for the main and recovery group were dissected, rinsed with PBS and lysed in T-PER™ tissue protein extraction reagent (Thermo Scientific) in the presence of 1× Halt™ Protease and Phosphatase Inhibitor Cocktail (Thermo Scientific). Tissue homogenization was accomplished by taking advantage of the Qiagen TissueLyser II Sample Disruption/Homogenizer *System* using 3 mm tungsten carbide beads (Qiagen). Following centrifugation (10,000 ×*g*, 10 min), protein supernatant concentrations were determined by Pierce™ BCA Protein Assay kit (Thermo Fisher Scientific). All samples were then diluted to 0.67 μg/mL in 1× ELISA sample diluent buffer (Millipore). Enzyme-linked immunosorbent assay (ELISA) analysis was performed in triplicates for each sample using the rat Lcn2/NGAL ELISA kit (Sigma), according to the manufacturer's instructions. The data are reported as ng of Lcn2 *per* mg of lung tissue, based on the standard curve for Lcn2 provided with the kit.

2.13. Statistical analysis

Copper levels in the different organs were analysed by 2-way ANOVA using Sidak's multiple comparison test. Clinical pathology parameters were log transformed and analysed by 2-way ANOVA using Tukey's multiple comparison test. Benchmark doses (BMD) and their one-sided lower and upper 95%-confidence limits (BMDL and BMDU, respectively) were estimated using PROAST (Gosens et al., 2015; idem, 2016). A benchmark response (BMR) of5% change was chosen for organ and body weight endpoints and a BMR of 100% for cell counts and BALF clinical chemistry. Differential cell counts were analysed as clustered quantal data, *i.e.*, as a number within a sample of 400 cells. No defaults are available for this type of response, therefore the BMR was set to a 20% extra fraction based on expert judgment. For the (ordinal) histopathology data, the BMR was set to 50% risk (EC_{50}), indicating the concentration at which the average animal develops the considered lesion of a predefined severity (Slob, 1999; Slob et al., 2014). Potency differences due to coating with PEI or ASC were analysed using the BMD approach including a covariate for coating (Slob, 2002). BMD plots are provided in the Supplementary information, Figs. S4–S17.

3. Results

3.1. Characterization of aerosols of surface modified CuO NPs

Although the CuO NPs have a primary particle size of 10 nm (mode, 9.2–14 nm – first and third quartile respectively) based on TEM analysis (Gosens et al., 2016), the CuO-PEI aerosol has a MMAD of 1.27 μm and geometric standard deviation (GSD) of 2.01 and the CuO-ASC aerosol has a MMAD of 1.17 μm and GSD 2.14. It is a well-known phenomenon for NPs to aggregate/agglomerate when dispersed in air, due to their dynamic motion and high surface energy, especially in the aereosolisation process employed here using a spray nozzle (Grassian et al., 2007, Eslamian and Ashgriz, 2007).

Using the computational Multiple-Path Particle Dosimetry (MPPD) model (software version 3.04, www.arra.com/mppd) (Anjilvel and Asgharian, 1995), the pulmonary deposition fraction for CuO-PEI was estimated to be 0.045 and the tracheobronchiolar fraction 0.096 for a 17.5 mg/m^3 aerosol with a density of 6.3 g/cm^3 (Suppl. Fig. S18). After exposure for 3 h per day for 5 consecutive days using a rat inhalation rate of 0.01 m^3/h, the pulmonary plus tracheobronchiolar load for CuO-PEI was estimated to be 0.37 mg. Given that both aerosols have very comparable MMAD and GSD, the pulmonary deposition fraction for CuO-ASC was estimated to be very similar to CuO-PEI, namely 0.046 and the tracheobronchiolar fraction 0.091. This results in a total lung load for CuO-ASC of 0.43 mg after exposure to 20.9 mg/m^3 for 3 h per day for 5 days. The prepared CuO-PEI and CuO-ASC stock suspensions (10 mg/mL) for aerosol generation were checked for endotoxin content. The CuO-PEI suspension contained less than the lowest detectable level of 3 IU/mL (0.3 IU/mg NPs). In addition, for the aerosol generation, the stock suspensions were diluted 5 times resulting in less than 0.06 IU/mg endotoxin content. To estimate the possible endotoxin level *per* rat we assumed that the endotoxin is associated with the CuO NPs. In the top dose group, rats are exposed for 5 days, 3 h per day to 17 mg/m^3 aerosol generated from the 2 mg/mL suspension. At day 6, after some clearance has already occurred, this resulted in a lung burden of 8.4 μg copper. The total amount of endotoxin *per* rat is estimated to be 0.0005 IU. For CuO-ASC, with a measured endotoxin level in the suspension of <4.5 IU/mL and a lung burden of 8.7 μg copper, this results in very low levels (0.09 IU/mg and 0.0008 IU *per* rat).

The static dissolution of CuO PEI and CuO ASC NPs was assessed in lung simulant fluid, *i.e.*, Gamble's solution and artificial lung lining fluid (ALF) and the ratio Cu^{2+} ion *versus* CuO NPs was determined by ICP-OES at 1 and 24 h (Table 1). As a reference 10 mL of a 100 mg/L CuO dispersion was used. Both CuO PEI and CuO ASC NPs showed a strong dependence on pH and the presence of amino acids complexing media.

Table 1
Dissolution of CuO nanoparticles in Gamble's solution and artificial lysosomal fluid (ALF) determined by ICP-OES.

		CuO tot* (ppm)	Cu^{2+} (ppm)	Cu^{2+}/CuO ratio (%)
Gamble's pH 7.4	CuO ASC_1h	122,79 ± 1,35	8,77 ± 0,05	7,1
	CuO ASC_24h	123,24 ± 1,10	10,82 ± 0,08	8,7
	CuO PEI_1hr	127,44 ± 0,92	5,40 ± 0,02	4,2
	CuO PEI_24hr	123,11 ± 0,74	9,44 ± 0,07	7,7
ALF pH 4.5	CuO ASC_1h	121,16 ± 0,19	96,19 ± 0,07	79,4
	CuO ASC_24h	120,97 ± 0,31	96,78 ± 0,12	80,0
	CuO PEI_1hr	120,41 ± 0,12	53,13 ± 0,09	44,1
	CuO PEI_24hr	123,52 ± 0,17	95,54 ± 0,17	77,3

Total concentration of CuO, calculated as: Cu (conc)/MW (Cu) * MW (CuO).

3.2. Evaluation of pulmonary impact of CuO NPs

The short-term inhalation study protocol was applied as described previously (Gosens et al., 2016), with a few modifications. The study design is presented in Suppl. Fig. S1. In brief, toxicological parameters were assessed one day after the final exposure (on day 6) and after a recovery period of 22 days (*i.e.*, study day 27, recovery group). Each group consisted of 5 animals. Groups for organ burden analysis consisted of 4 animals.

3.3. Histopathological evaluation of lungs, lymph nodes and nasal cavity

Exposure to CuO-PEI or CuO-ASC did not lead to mortality, or changes in the behaviour of the animals during the exposure and recovery period. No treatment-related histopathological changes were visible in the liver, spleen, kidneys, and brain (data not shown). Exposure-related histopathological findings after treatment with both CuO-PEI and CuO-ASC were noted in the lung of all treatment groups (Suppl. Tables S2 and S3 resp.), in the mediastinal lymph nodes (Suppl. Tables S4 and S5, respectively), and in the nasal cavities (Suppl. Tables S6 and S7, respectively). A minimal to slight increased incidence in alveolar macrophages was observed in the lower dose groups (at 0.6–6.0 mg/m^3 for CuO-PEI and at 0.8–2.3 mg/m^3 for CuO-ASC) most likely representing the phagocytic response of the alveolar macrophages to particulate material. At higher doses, this process progressed into an alveolar and/or interstitial inflammatory response consisting of abundant granulocytes and/or macrophages which was dose-dependent (at 0.6–17.3 mg/m^3 CuO-PEI and at 2.3–21.8 mg/m^3 CuO-ASC). The inflammatory response was accompanied by the presence of cell debris in the alveoli. In addition, at all doses of CuO-PEI and at 7.5–21.8 mg/m^3 CuO-ASC alveolar and/or bronchiolar hypertrophy/hyperplasia was observed (Suppl. Tables S2 and S3, Fig. 1A–D). After a recovery period of 22 days, a minimal (CuO-ASC) to slight (CuO-PEI) increase in alveolar macrophages was still observed and minimal bronchiolar hypertrophy/

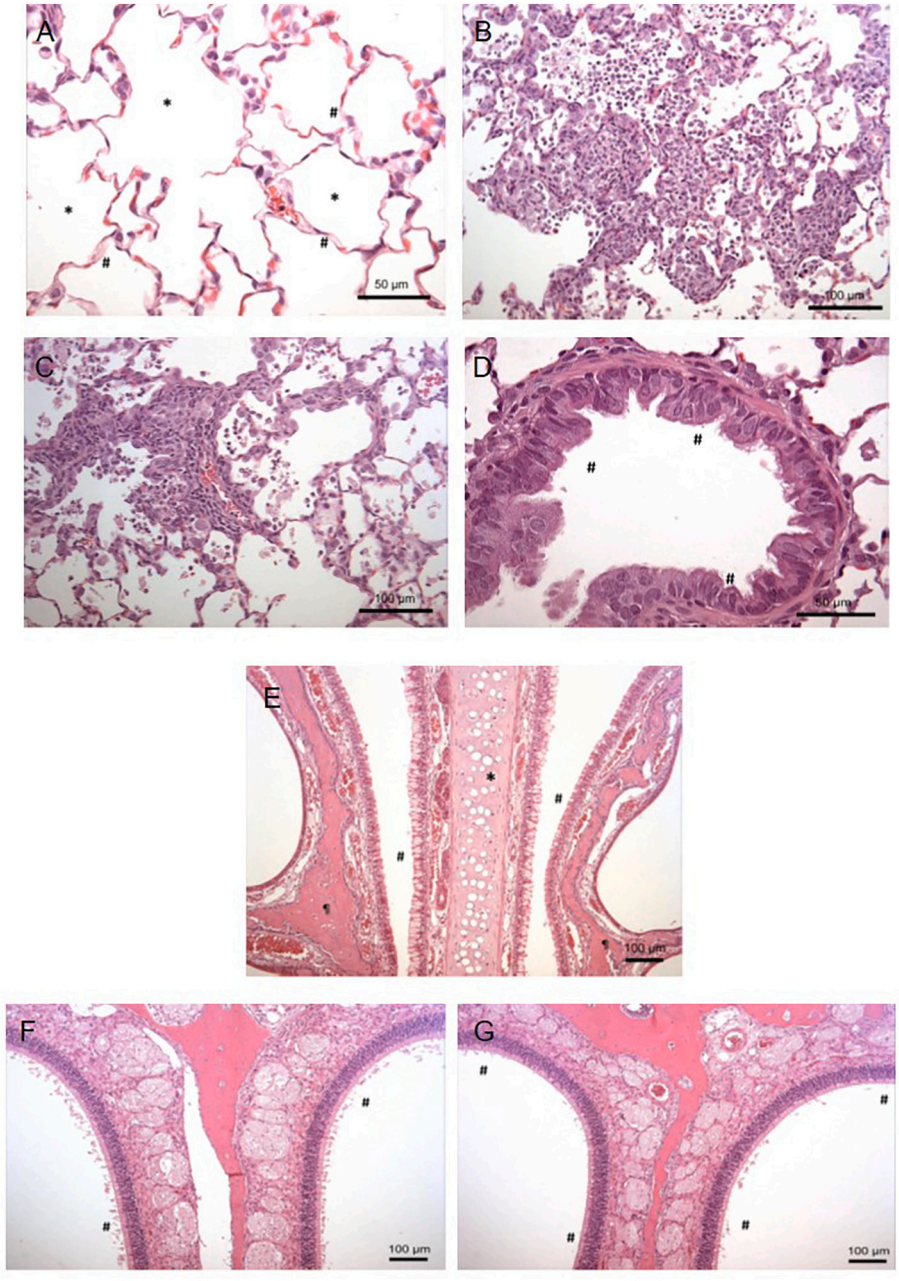

Fig. 1. Histopathology of the lung and nose following short-term inhalation exposure. (A) clean air exposure for 5 consecutive days, day 1–5. Detail of air containing alveoli (*) and septa (#). (B) CuO-PEI, day 6 (exposure dose 17.3 mg/m^3 for 5 consecutive days, day 1–5). (C) CuO-ASC, day 6 (exposure dose 21.8 mg/m^3 for 5 consecutive days, day 1–5). Note presence of alveolar and interstitial inflammation with cellular debris in alveoli in B and C. (D) CuO-PEI, day 6 (exposure dose 17.3 mg/m^3 for 5 consecutive days, day 1–5. Detail of bronchiolar hypertrophy (#) in the lung. (E) Nasal epithelium after clean air exposure day 6 (clean air exposure for 5 consecutive days, day 1–5). Note presence of normal nasal epithelium (#) including goblet cells, cartilage in nasal septum (*) and nasal bone (¶). (F) Nasal cavity after clean air exposure. Note regular arrangement of nuclei of the cells in the epithelial cell layer. Note normal nasal epithelium (#). (G) Nasal cavity after CuO-PEI, day 6 (exposure dose 17.3 mg/m3 for 5 consecutive days, day 1–5). Note slight disorganization of the cell nuclei in the epithelium (#). Refer to the supplement for a quantification of the histopathological findings.

hyperplasia was noted in two animals. This is indicative of ongoing clearance of CuO NPs by alveolar macrophages accompanied by restoration of the normal lung architecture. The alveolar and interstitial inflammation was resolved, while bronchiolar and alveolar epithelium recovered (Suppl. Tables S2 and S3).

Furthermore, a dose-dependent increased incidence and severity of histiocytosis was observed in the paracortical region of the mediastinal lymph nodes after both treatments (Suppl. Figs. S19B–C). Note that some histiocytosis is also observed in clean air controls (Fig. S19A). The potencies of both types of NPs in causing histiocytosis when assessed using the BMD approach, is equal (the confidence intervals BMDU-BMDL for PEI and ASC overlap, 2.1–5.6 mg/m^3). After the CuO-free period of 22 days, for both coatings no histiocytosis occurred, suggesting full recovery (Suppl. Tables S4 and S5).

In a few animals (1 animal at 1.8 and 6.0 mg/m^3 CuO-PEI, and 4 animals at 21.8 mg/m^3 CuO-ASC of which 1 animal after recovery) disorganization of the olfactory epithelium was observed (Fig. 1E–G). This disorganization represented atrophy, the presence of pycnotic nuclei and unstructured epithelial cell layers, or a combination of these features. Based on the relatively low severity of the changes and the fact that some disorganization of the epithelium remained only in 1 animal in the recovery group, while effects generally had resolved, this finding seems of minimal toxicological significance (Suppl. Tables S6 and S7). The remainder of the recorded findings in liver, spleen and kidneys were within the range of background histopathology in rats of this strain and age, and not considered to be treatment-related. No hematological abnormalities were noted.

3.4. Benchmark dose modelling of the lung impact of CuO aerosols

Exposure to both types of modified CuO NPs induced a dose-dependent increase in several BALF markers such as the total cell number (Fig. 2A–B) and LDH, indicative of cell damage (Fig. 2C–D).

We also observed an increase in the number of macrophages and neutrophils, as well as in the presence of total protein, ALP, NAG, and GGT (data not shown). The nature of the toxicological response in rats after exposure to CuO-PEI and CuO-ASC was found to be similar with the same markers affected. Using the BMD approach, the potency difference between the two aerosols was analysed (Suppl. Table S8). The only difference in response to CuO-ASC and CuO-PEI is that exposure to CuO-PEI led to bronchiolar hypertrophy at a lower dose compared to CuO-ASC, while CuO-ASC led to alveolar hypertrophy at a lower dose compared to CuO-PEI (Fig. 3). This difference in alveolar *versus* bronchiolar hypertrophy could be due to slight differences in lung deposition between positively and negatively charged aerosols. The deposition according to MPPD modelling did not result in a difference in the deposited fraction in alveoli *versus* the bronchial area (see above). However, the MPPD model does not take differences in particle charge into account while this could influence the deposition.

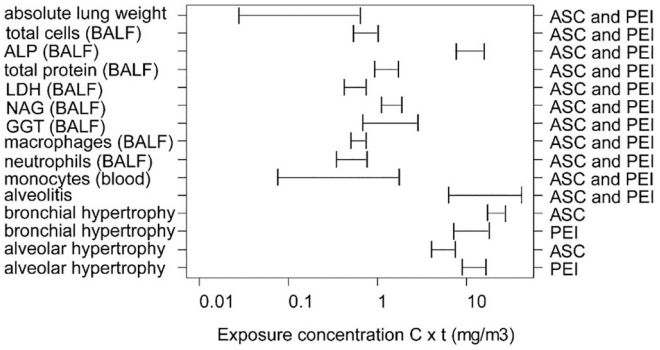

Fig. 3. Summary of benchmark dose (BMD) confidence intervals for lung toxicity markers after exposure to CuO-PEI and CuO-ASC aerosols expressed as 3-h exposure equivalents. When the statistical analysis showed that there is no difference in the potency between the aerosols, a single BMD confidence interval is derived and plotted for ASC and PEI (ASC and PEI on the right side of the figure).Potency differences were observed only for bronchiolar and alveolar hypertrophy, based on histopathological findings. This is indicated with a separate BMD confidence interval for ASC and PEI.

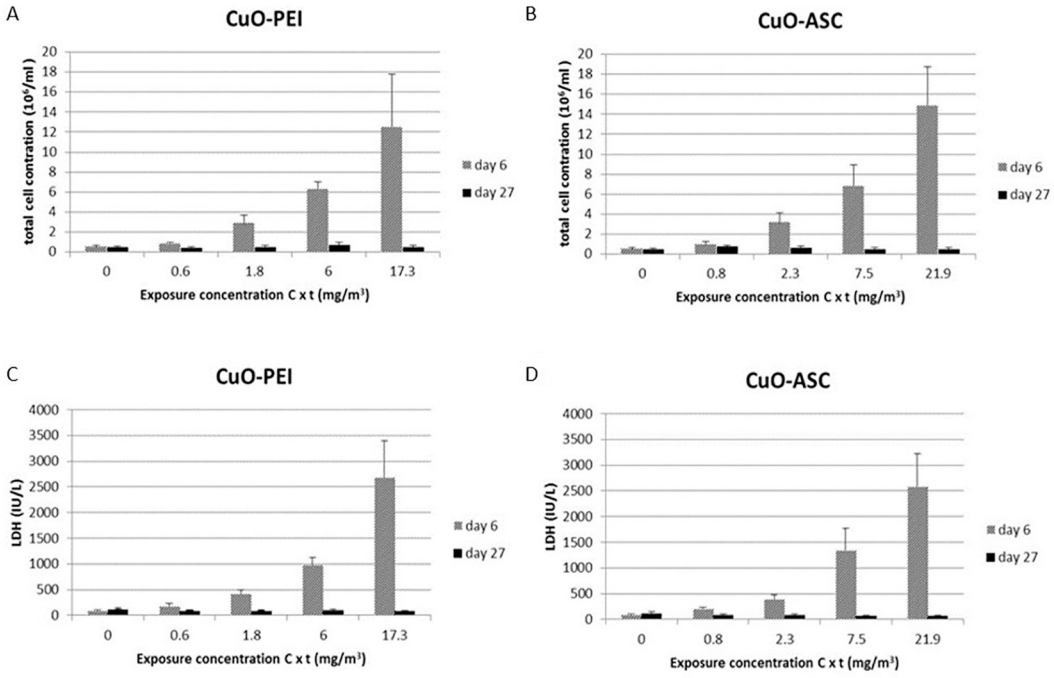

Fig. 2. BALF analysis reveals inflammation and cellular damage (n = 5 per group). (A) Total cell concentration after exposure to CuO-ASC, (B) total cell concentration after exposure to CuO-PEI, (C) LDH after exposure to CuO-ASC, and (D) LDH after exposure to CuO-PEI at 1 day after exposure (day 6) and after a recovery period of 22 days (*i.e.*, day 27).

3.5. Organ burden analysis at day 6 and day 27 after exposure

No exposure related increases above background Cu levels were observed at day 6 or day 27 following exposure to either CuO-PEI or CuO-ASC (Suppl. Fig. 20) in organs other than in the lung, similarly to what has been found for the pristine CuO NPs (Gosens et al., 2016). In the lung, the increasing exposure (as 3-h exposure equivalents) resulted in an increase in lung burden at day 6. After subtracting the background Cu levels, exposure to the top dose CuO-PEI (3-h exposure equivalent 17.5 mg/m^3) resulted in a lung burden of 32.6 μg copper *per* gram dried lung weight at day 6. Based on the actual average dry lungs weight of 260 mg, this resulted in a total lung burden of 8.4 μg copper. A similar calculation results in a lung burden of 32.4 μg copper *per* gram dried lung weight after exposure to the top dose of CuO ASC (3-h exposure equivalent 20.9 mg/m^3) and a total lung burden of 8.7 μg copper (actual average dried lung weight 270 mg). Within the 21-day recovery period, Cu was completely cleared from the lung (Fig. 4A–B). The lung burden following a 3-h exposure to CuO-PEI and CuO-ASC was compared to the 6-h exposure to CuO pristine by transforming the 3-h exposure to a 6-h exposure following the C × T concept and expressing it on a log to log scale. Both exposure to CuO-PEI and CuO-ASC resulted in a similar lung burden compared to CuO pristine (Fig. 4C). A true quantitative comparison is not possible, since the rat strain and age/body weight of the rats were different between the studies for PEI/ASC (the present study) and pristine CuO NPs (Gosens et al., 2016). Unfortunately, an infection problem at the breeder of the strain used in the previous study with pristine CuO NPs prevented us from using the same rat strain in the present study.

3.6. Microarray analysis of gene expression changes in rat lungs

Next, we performed transcriptomics analyses of total lung tissues of exposed and control rats. We identified a total of 654 significant DEGs, almost entirely pertaining to rats sampled after exposure (Suppl. Fig. S21A), *i.e.*, at day 6, comparatively to rats enduring exposure plus recovery (at day 27) (Suppl. Fig. S21B), which is in accordance with our previous work on rats exposed to unmodified CuO NPs (Costa et al., 2018). However, in contrast with the preceding study, the number of juxtaposed DEGs between treatments is much higher and there is a more even distribution of up- and downregulated genes. The highest fold change (FC ≈ 70) pertains to *lcn2* encoding lipocalin 2, a protein involved in the sequestration of iron, in animals exposed to CuO-ACS (high dose) (Suppl. Table S9). This gene was also overexpressed in the remaining treatments following exposure (but not recovery) (FC ranging from about 11–16). This was followed by *defb3* encoding the antimicrobial peptide beta-defensin 3 in rats exposed to CuO-PEI (low dose). Interestingly, the D-box binding PAR bZIP transcription factor (*dpb*), which regulates the expression of some drug-metabolizing cytochrome P450 (CYP) enzymes was consistently found to be the most upregulated gene in CuO-ASC exposed animals (FC ≈ 20) (Suppl. Table S9). Downregulation was strongest for *gp2* encoding glycoprotein 2 (a pathogen-binding protein involved in innate immune responses) in CuO-PEI exposed animals (low dose, after recovery) (FC ≈ − 6). This was followed by the serpin B10 encoding gene (*serpinb10*) in CuO-PEI exposed animals (high dose) and the CYP encoding gene *cyp26b1* in CuO-ASC exposed animals (low dose), both immediately after exposure (day 6) (FC ≈ −5) (Suppl. Table S9). To provide validation of these data at the protein level, we focused on the top-most affected gene *lcn2*, encoding lipocalin 2 (Lcn2). To this end, lung tissue samples from rats exposed to the highest dose of CuO-PEI or CuO-ASC at day 6 and rats following exposure plus recovery (at day 27) *versus* control were subjected to analysis by ELISA. As shown in Suppl. Fig. S20, Lcn2 levels were markedly elevated at day 6 both for CuO-PEI and CuO-ASC exposed groups and were normalized at day 27.

Hierarchical cluster analysis (Fig. 5) of all DEGs and treatments showed a consistent differentiation between exposure and recovery, while differences between the two surface modifications were scant, regardless of dose (see dendrogram at the top of the heatmap). Gene ontology associated pathways with two major clusters of DEGs that included most of the probes (Benjamini-adjusted $p \approx 0$) were identified (Fig. 5). The first (upper) cluster includes genes that affect steroid metabolism (4 genes) and basal metabolic pathways (16 genes) as the top-most statistically significant. The second cluster includes major immune response pathways, the top-most being IL-17 signaling (11

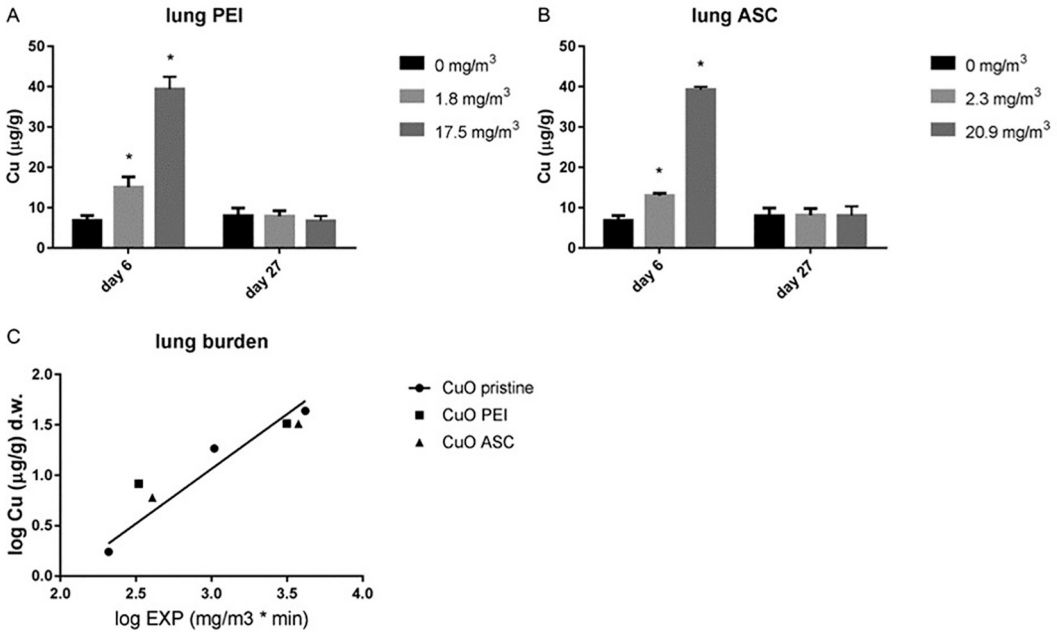

Fig. 4. Organ burden analysis (n = 4 per group). Lung Cu burden (in μg/g organ dry weight) was assessed 1 day after the last exposure (day 6) and after a recovery period of 22 days (day 27) in control animals and in animals exposed to 1.8 mg/m^3 and 17.5 mg/m^3 CuO-PEI (A) or 2.3 mg/m^3 and 20.9 mg/m^3 CuO-ASC (B), for 5 consecutive days. (C) Lung burden comparison between studies using pristine CuO (Gosens et al., 2016) and modified CuO (the present study). * indicates significant differences compared to control (2-way ANOVA with Sidak's multiple comparisons test, $p < 0.05$).

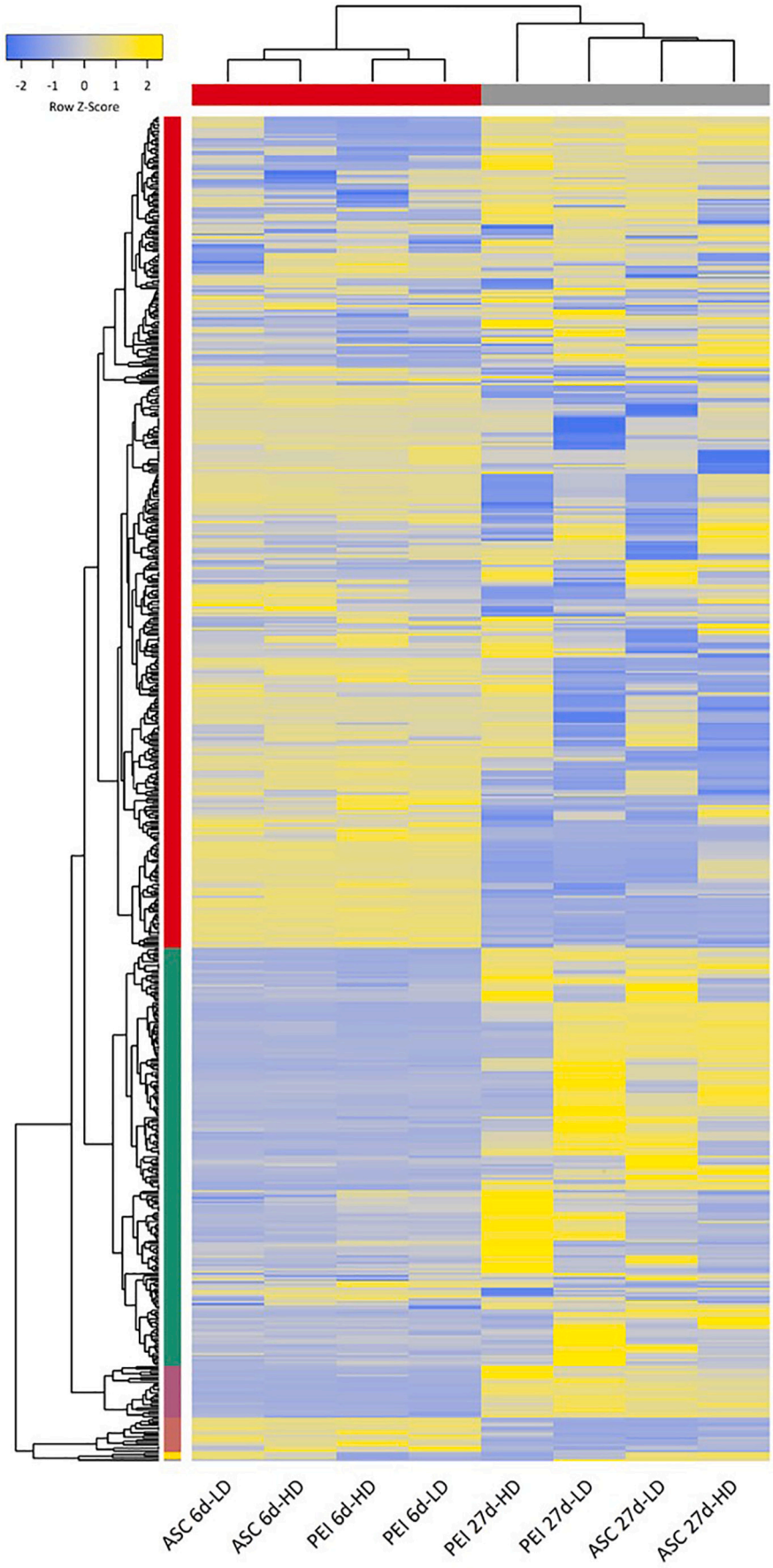

Fig. 5. Transcriptomics analysis of rat lungs following exposure to CuO NPs. Heatmap comprising all 654 differentially expressed genes (DEGs), normalized by row (*i.e.*, by gene). Hierarchical clustering of genes (dendrogram to the left) and experimental treatments (upper dendrogram) was done using Euclidean distances and complete linkage analysis. The two major clusters of DEGs are denoted (1) and (2). The upper cluster includes genes that affect steroid metabolism (adj. p-value: 7.867333e-06) and metabolic pathways (adj. p-value: 2.241742e-03), while the lower cluster includes immune related pathways, such as IL-17 signaling (adj. p-value: 1.449865e-06) and cytokine-cytokine receptor interactions (adj. p-value: 2.094660e-06).

genes) and cytokine-cytokine receptor interaction pathways (17 genes).

Furthermore, pathway analyses using IPA yielded strong activation (z-score > 2) of canonical pathways related to inflammation and cell cycle in samples collected at day 6, *i.e.*, immediately after exposure, with no evident differences between CuO-PEI and CuO-ASC (Fig. 6A). The most significantly deactivated pathway, in all 6-day rats (albeit highest in the PEI group) was cell cycle: G2/M DNA damage checkpoint regulation (re-activated after recovery), which is in agreement with the activation of cell cycle- and mitogenesis-related pathways. The segregation between exposure and recovery treatments, as well as the overall similarity between CuO-PEI and CuO-ASC, was even more obvious when comparing disease and function pathways.

Here we found pathways pertaining to innate immunity and cell proliferation (including lung cancer cells, forming a distinct cluster of pathways) consistently activated after exposure and deactivated after recovery. Five out of sixteen pathways were related to granulocyte (especially neutrophil) mobilization, while three pathways were related to cancer cell proliferation. Notably, immune response and cell proliferation networks were linked by the upregulation of several common genes as illustrated in Fig. 7. Among these are the genes encoding epithelial cell transforming sequence 2 (ect2) and the C—C motif chemokine ligand 2 (ccl2) (Suppl. Table S10).

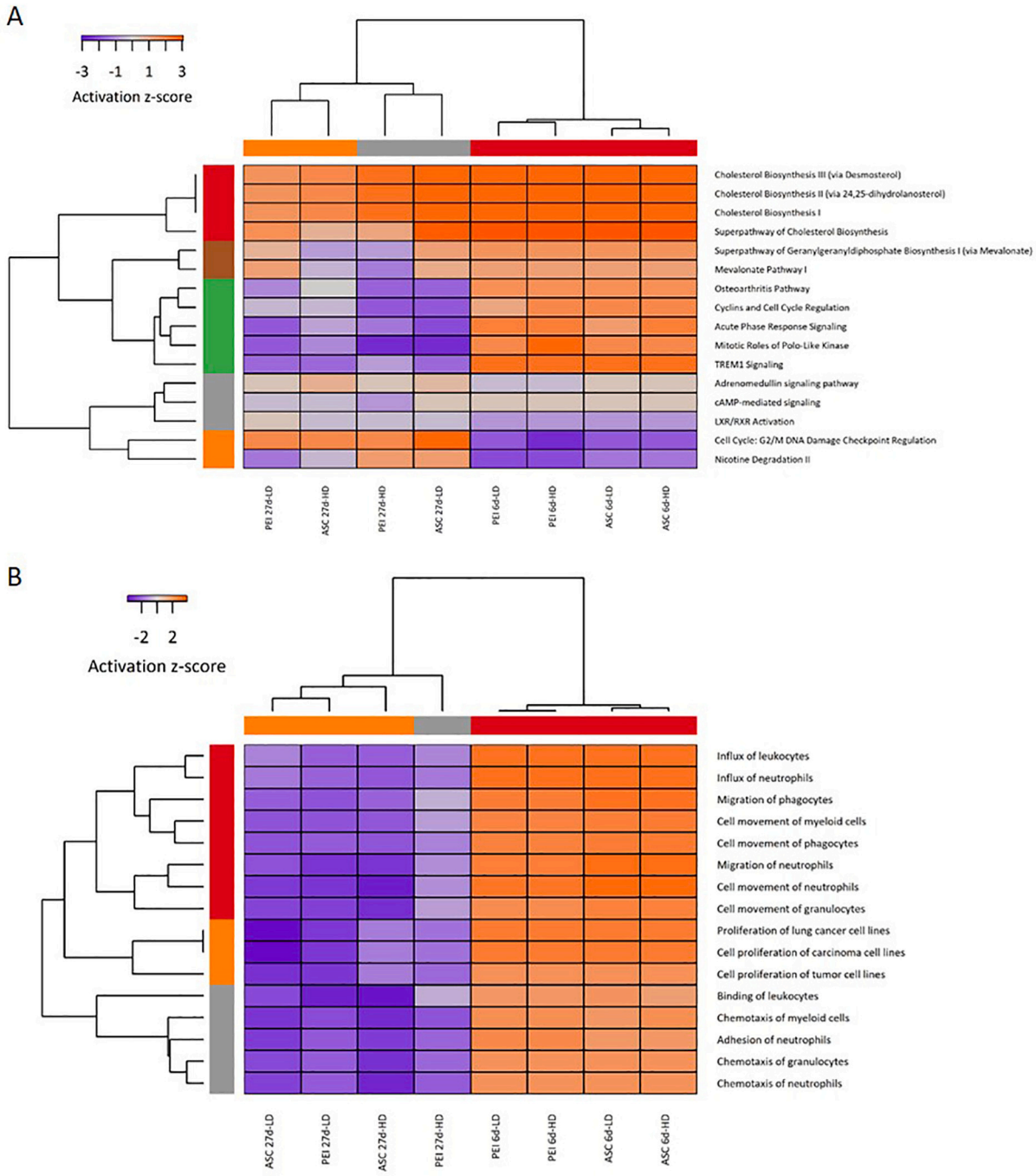

Fig. 6. Hierarchical clustering of molecular pathways as determined by Ingenuity Pathway Analysis (IPA) of the transcriptomics data combining all experimental conditions (exposure and recovery). (A) Cluster analysis heatmap for 'canonical pathways'. Clustering of pathways (left dendrogram) and treatments (upper dendrogram) was done with Euclidean distances and complete linkage computed from activation scores. (B) Cluster analysis heatmap for 'diseases and functions'. Clustering of pathways (left dendrogram) and treatments (upper dendrogram) was obtained as above.

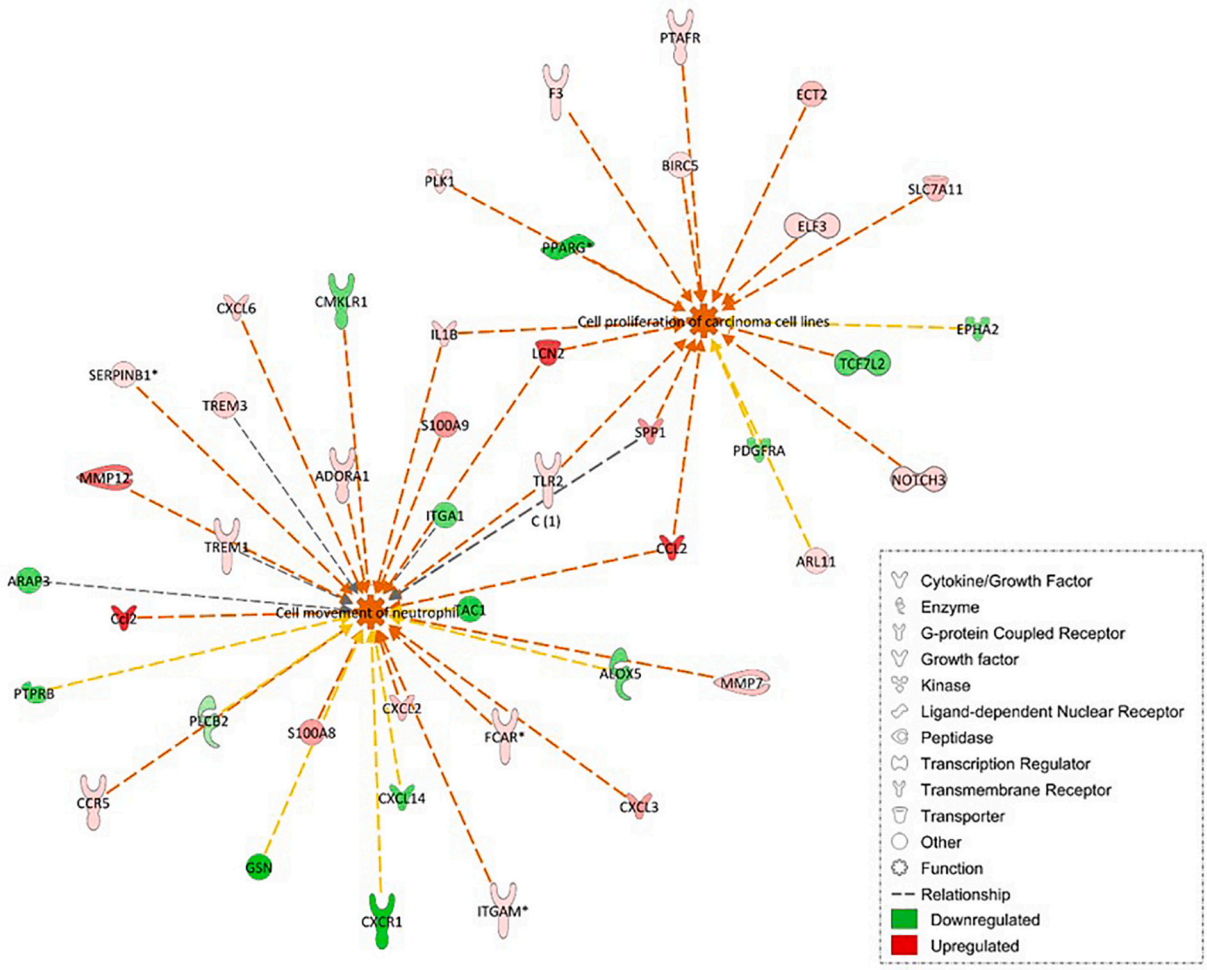

Fig. 7. Network analysis. The figure depicts the network associations between the two 'diseases and functions' pathways related to cell proliferation and immune responses (refer to main text). The probes corresponding to the two most significantly activated pathways in the lungs of animals exposed to the high dose of CuO-PEI (day 6) are shown. Note that the genes encoding lipocalin 2 (*lcn2*) and C—C motif chemokine ligand 2 (*ccl2*) are among those that connect the two networks in question; both are upregulated.

4. Discussion

The present study aimed at comparing the *in vivo* effects of exposure through inhalation to the most and least cytotoxic surface-modified CuO NPs (CuO-PEI and CuO-ASC, respectively), according to our previous *in vitro* study using a macrophage-like cell line (Líbalová et al., 2018). We determined BALF inflammatory and cell damage markers, conventional histopathological endpoints and assessed gene expression changes by genome-wide microarray analysis. In brief, CuO-PEI and CuO-ASC displayed the same effects in terms of the type of toxicity endpoints that are affected following short-term inhalation exposure in a rat model. This, therefore, disproves our hypothesis that differences in surface coatings resulting in a positive or negative surface charge respectively, affects the pulmonary toxicity of CuO NPs.

We noted that the lung burden of Cu *per* gram dried lung weight at day 6 was very similar for both CuO-PEI and CuO-ASC, and following a 21-day recovery period, Cu was completely cleared from the lungs. Furthermore, our detailed histopathological examinations revealed exposure-related changes in the lungs of all treatment groups after exposure to both CuO-ASC and CuO-PEI. The alveolar and interstitial inflammation was resolved after a 21-day recovery period (*i.e.*, at day 27 of the study). No treatment-related histopathological changes were visible in the liver, spleen, kidneys, or brain. The response to CuO-PEI and CuO-ASC was found to be similar with respect to BALF analysis, which indicated a dose-dependent increase in the total cell number and LDH (a marker of plasma membrane disintegration). The very low levels of endotoxins detected on the NPs are unlikely to have contributed to these effects.

By applying the statistical method of the BMD approach, we could make a fair comparison of the toxic effects on the entire exposure concentration range and assess potency differences between the two types of surface modified CuO NPs. BALF total cell number, differential cell counts and cell damage markers, absolute wet lung weights and the histopathology results were analysed in this fashion. The only difference in the pulmonary response was noted in the histopathology assessment. Exposure to CuO-PEI led to bronchiolar hypertrophy at a lower (benchmark dose) compared to CuO-ASC, while CuO-ASC led to alveolar hypertrophy at a lower dose compared to CuO-PEI. This may have been a consequence of the slight difference in the dose distribution between these two lung regions due to the electrostatic forces. As stated before, PEI coated CuO NPs had a positive ζ potential in water, while ASC coated NPs had a negative ζ potential. The aerosol was generated from a stock suspension in water. This, however, did not affect the overall dose in the lung, which explains why the less region specific BALF analyses did not show any difference between groups of rats exposed to CuO-ASC or CuO-PEI. Overall, the gene expression analysis corroborated these findings. Hence, CuO-PEI and CuO-ASC were found to elicit changes in pathways related to inflammation and cell proliferation, and these gene expression changes were largely restored to control levels following the 21-day recovery period.

The microarray results obtained herein are concordant with our findings in an earlier study in which rats were exposed to pristine CuO NPs (Costa et al., 2018). Thus, molecular pathways related to inflammation and cell proliferation were significantly activated during exposure and largely returned to control levels during recovery. However, the present study also revealed that CuO-PEI triggered the deactivation of DNA damage checkpoint related genes, which is a risk factor for the onset of neoplasia (Calonge and O'Connell, 2008). Considering that Cu is a known genotoxicant and is even suspected to be a mutagen (Prá et al., 2008), our study suggests that pulmonary exposure to CuO NPs could potentiate the risk of developing neoplastic disease.

Indeed, in a recent, comprehensive study, Rossner et al. (2020) employed next generation sequencing protocols and determined gene expression changes in the lungs of mice exposed to inhalation of CuO NPs (8×10^5 NPs/m^3) for up to 3 months. Notably, at three months of exposure, the authors observed dysregulation of several genes potentially implicated in carcinogenesis. In the present study, we found evidence for the dysregulation of drug metabolism-related genes, especially in animals exposed to CuO-ASC, which may be interpreted as an attempt by the cells to eliminate the capping agent. It is worth noting that while ascorbate is an important physiological antioxidant it can also exert prooxidant effects in the presence of free transition metal catalysts (Frei et al., 1989). Thus, capping agents are not necessarily innocuous, and the toxicity of NPs may result from an interplay between particles and surface coatings, as shown previously (Líbalová et al., 2018).

The present findings confirmed that the genes encoding CCL2 and ECT2 are significantly elevated in response to CuO NPs, in line with previous work (Costa et al., 2018). Furthermore, we found that among the 654 significant DEGs, the gene encoding lipocalin 2 displayed the greatest FC (almost 70-fold upregulation in rats exposed to CuO-ACS). These findings were validated by ELISA analysis of homogenized lung tissue samples from the high-dose group. Notably, *lcn2* was also overexpressed in rats exposed to unmodified CuO NPs in our previous study, but FCs were lower (≈19) (Costa et al., 2018). Lipocalin 2, also known as oncogene 24p3 or neutrophil gelatinase-associated lipocalin (NGAL), is an iron-binding protein that serves to complement the transferrin system (Kaplan, 2002). While LCN2/NGAL was originally identified as a component of neutrophil granules, it is also expressed in macrophages and in epithelial cells of the respiratory and gastrointestinal tracts. Recent studies suggested that LCN2 promotes bacterial clearance by macrophages, thereby suppressing inflammation (Toyonaga et al., 2016). We studied whole lung tissue here, yet it is relevant to ask whether *lcn2* upregulation occurs in macrophages, neutrophils, and/or epithelial cells in exposed animals. Kodali et al. (2013) suggested, based on transcriptional profiling, that common mechanisms for the dysregulation of innate immunity exist by virtue of shared recognition pathways between certain NPs and pathogenic bacteria.

Our previous work showed that CuO NPs, if dispersed in amino acid enriched media, tend to dissolve rapidly, even at high pH (the pH of DMEM is around 8), despite surface coating with PEI and ASC (Baldissarri and Costa, 2016; Líbalová et al., 2018). This is due to the known copper complexation ability of amino acids present in biological media that alter the dissolution equilibrium leading to an increase of the dissolved fraction (Borsook and Thimann, 1932; Gale and Winkler, 1977; Garnier and Tosi, 1975). Furthermore, pristine (non-modified) CuO NPs triggered the upregulation of *mt1a* and *mt2a* in the lungs of rats (Costa et al., 2018). Strauch et al. (2017) studied the cytotoxicity of nano- and micro-sized CuO NPs as compared to $CuCl_2$ in human bronchial epithelial BEAS-2B cells and human lung adenocarcinoma A549 cells coupled with gene expression analysis and found a strong induction of the metallothionein (MT) genes, *MT1X* and *MT2A*. Hanagata et al. (2011) also noted upregulation of a host of MT genes in A549 cells exposed to CuO NPs. Similar upregulation of MT genes was presented in a recent transcriptomics report by Boyadzhiev et al. (2021), where mouse lung epithelial cells from MutaMouse were exposed to varying doses of CuO NPs, CuO MPs and $CuCl_2$ for different periods of time. We showed that ZnO NPs elicit the upregulation of several MT genes in primary human monocyte-derived macrophages (Tuomela et al., 2013). In the present study, the most significantly overexpressed MT was *mt1a*, attaining FC = 2.83 in animals exposed to a high dose of CuO-ASC (and FC = 2.79 for the low dose treatment), whereas CuO-PEI reached FC = 2.28 and 2.15 (low and high dose, respectively). The expression of MTs returned to control levels after recovery (day 27). Overall, the induction of MT genes seems to serve as a common cellular response to metallic nanoparticles that readily dissolve.

Our recent transcriptomics studies of rat lungs following pulmonary exposure to pristine CuO NPs failed to demonstrate significant perturbations of pathways related to oxidative stress (Costa et al., 2018). Similarly, in the present study, oxidative stress genes or pathways were seemingly not affected. However, *in vitro,* the pathway perturbation following exposure to CuO NPs is shown to exhibit an incremental transition involving cellular stress (heat shock genes) and defense mechanism pathways at low dose and early post-exposure time points to oxidative stress, autophagy and early DNA damage pathways at moderate doses and, DNA damage and cytotoxicity pathways at high dose/late post-exposure time points (Boyadzhiev et al., 2021. Also, *in vivo*, the post-exposure time points at which the sampling is conducted plays an important role, which may explain why oxidative stress associated pathways were not observed in the present study. Additionally, *in vivo*, tissue anti-oxidative capacity may protect from mounting oxidative stress. Thus, even though oxidative stress is assumed to be important, its role in CuO NP-induced toxicity *in vivo* remains uncertain. Interestingly, Saporito-Magriñá et al. (2018) have recently provided evidence that while the cellular antioxidant glutathione (GSH) protects cells from Cu-mediated cytotoxicity this was independent of its reactive thiol group. The authors could show that cell death is driven by the interaction of cuprous ions with proteins which impairs protein folding and promotes protein aggregation. Consequently, cells reacted to Cu by mounting a heat shock response leading ultimately to cell death (Saporito-Magriñá et al., 2018). Indeed, in a recent proteomics-based study, we observed that CuO NPs triggered the upregulation of proteins involved in heat shock responses in the human monocytic leukemia cell line THP-1 (Tarasova et al., 2017). Thus, a take-home message from these studies is that while transcriptomics-based approaches are exquisitely sensitive, protein expression changes are also important (Costa and Fadeel, 2016).

Our comparative analysis of activation of the molecular pathways related to inflammation and cell proliferation showed few differences between CuO-ASC and CuO-PEI at low or high doses, which indicates a more significant impact of the NPs themselves, even though CuO-ASC were shown to be less cytotoxic than CuO-PEI when tested on mouse macrophages *in vitro* (Líbalová et al., 2018). Thus, one should exercise caution when attempting to extrapolate from *in vitro* assays (often based on a single cell type) to the *in vivo* situation where an interplay between different lung epithelial cells and immune cells take place. Nevertheless, the key factor which determines the outcome of CuO NP exposure is likely the fact that the NPs rapidly dissolve in the acidic environment of the lysosomal compartment of macrophages (Gosens et al., 2016; Zhang et al., 2018). Capping agents that prevent NP dissolution may mitigate their biological effects (Tuomela et al., 2013), but in the case of CuO-ASC and CuO-PEI, our studies show that both undergo dissolution in cell culture media (Ortelli et al., 2017; Líbalová et al., 2018). In the mouse macrophage assay (Líbalová et al., 2018), ASC and PEI coatings only modestly affected Cu dissolution, suggesting that the *in vitro* cytotoxicity is modulated by the interaction between coating agent and copper bioavailability and not copper levels insides the cells alone.

Our results indicate that effects of the initial surface characteristics of the CuO PEI (positively charged) and ASC (negatively charged) NPs, are mitigated by the environment encountered in the lung after the inhalation exposure resulting in similar adversity. A similar observation has been made when comparing TiO_2 NPs with an endogenous negative charge *versus* surface modified TiO_2 NPs with a positive charge (Wallin et al., 2017). In our study, the toxicity did not seem to be surface charge/

chemistry dependent. Looking to descriptors that potentially affect fate and toxicity in *in vivo* models such as the colloidal stability (degree of agglomeration) and metal ions release, we did not find significant differences between the two samples. In particular, the static dissolution data of both CuO PEI and CUO ASC NPs in lung simulant fluids showed a strong dependence from pH and the presence of amino acids complexing media. CuO-PEI NP dissolution needs more time to reach equilibrium, but after 24 h the ratio Cu^{2+}/CuO is the same (75%). In terms of NPs dispersability in water, CuO-ASC resulted the best dispersed sample (DLS-size ≈ 100 nm for CuO-ASC and ≈250 nm for CuO-PEI), if compared with naked CuO (DLS-size ≈ 1000 nm), but this effect is lost once NPs are aerosolised and agglomerate inside the aereosolisation chamber. Based on the results of the present study, a possible suggestion to overcome limits of the proposed safe-by-design strategy, is to explore inorganic coatings (*e.g.*, silica) that can limit the bioavailability of leached ions, acting as an entrapping matrix (Gardini et al., 2018).

5. Conclusions

Using a short-term inhalation protocol (Gosens et al., 2016; Costa et al., 2018), we found that the functionalized CuO NPs by ASC and PEI elicited a dose-dependent pulmonary inflammation and cell damage. Furthermore, transcriptomics analysis showed that pathways related to inflammation and cell proliferation were significantly activated. A small difference was found in CuO-PEI leading to bronchiolar hypertrophy at a lower (benchmark) dose compared to CuO-ASC, while CuO-ASC led to alveolar hypertrophy at a lower dose compared to CuO-PEI. This could be due to a difference in the dose deposition in these lung regions as a result of a differences in electric charges. Overall, no differences in the type of toxic effects or toxic potency in the lung could be established between the two surface coatings. This disproves our hypothesis that CuO-ASC NPs would be less toxic than CuO-PEI NPs per unit mass. Notwithstanding, our study has shown good concordance between conventional toxicity methods and the more sensitive microarray-based transcriptomics analyses of lung tissues.

Declaration of Competing Interest

The authors declare that they have no known competing financial interests or personal relationships that could have appeared to influence the work reported in this paper.

Acknowledgements

This work was supported by the SUN ('sustainable nanotechnology') project funded by the Seventh Framework Program of the European Commission (grant agreement no. 604305), and by the RIVM Strategic Research Program, the Netherlands (SPR, E/121504). P.M.C. acknowledges the support provided by national funds to UCIBIO through Fundação para a Ciência e Tecnologia (FCT, Portugal), ref. UIDB/04378/2020. S.H. acknowledges the support of the Health Canada Genomics Research and Development Initiative. The authors thank M. V. W. Wijnands, for the histopathological examinations, and E.H.J.M. Jansen, D.L.A.C. Leseman, C.M.R. Soputan, J. Rigters, S. Oude Hendrikman, P. K. Beekhof, B. Nagarajah, L.J.J. de la Fonteyne, T. Schouten, A. Gomersbach, H. Verharen, H.J. Heusinkveld, A.J.F. Boere, and P.H.B. Fokkens, all at RIVM, for their help with the animal experiments and for valuable technical assistance. The authors also thank D. Wu at Health Canada for assistance with the microarray analysis, and S. Ortelli for the thermographic analysis of the modified CuO NPs.

Appendix A. Supplementary data

Supplementary data to this article can be found online at https://doi.org/10.1016/j.impact.2021.100313.

References

Anjilvel, S., Asgharian, B., 1995. A multiple-path model of particle deposition in the rat lung. Fundam. Appl. Toxicol. 28 (1), 41–50.
Baldisserri, C., Costa, A.L., 2016. Electrochemical detection of copper ions leached from CuO nanoparticles in saline buffers and biological media using a gold wire working electrode. J. Nanopart. Res. 18 (96), 1–20.
Benjamini, Y., Hochberg, Y., 1995. Controlling the false discovery rate: a practical and powerful approach to multiple testing. J. R. Stat. Soc. B 57 (1), 289–300.
Borsook, H., Thimann, K.V., 1932. The cupric complexes of glycine and of alanine. J. Biol. Chem. 98 (2), 671–705.
Boyadzhiev, A., Avramescu, M.L., Wu, D., Williams, A., Rasmussen, P., Halappanavar, S., 2021. Impact of copper oxide particle dissolution on lung epithelial cell toxicity: response characterization using global transcriptional analysis. Nanotoxicology 28, 1–20.
Brenner, S.A., Neu-Baker, N.M., Caglayan, C., Zurbenko, I.G., 2016. Occupational exposure to airborne nanomaterials: an assessment of worker exposure to aerosolized metal oxide nanoparticles in semiconductor wastewater treatment. J. Occup. Environ. Hyg. 12 (7), 469–481.
Buchman, J.T., Hudson-Smith, N.V., Landy, K.M., Haynes, C.L., 2019. Understanding nanoparticle toxicity mechanisms to inform redesign strategies to reduce environmental impact. Acc. Chem. Res. 52 (6), 1632–1642.
Calonge, T.M., O'Connell, M.J., 2008. Turning off the G2 DNA damage checkpoint. DNA repair 7 (2), 136–140. https://doi.org/10.1016/j.dnarep.2007.07.017.
Cho, W.S., Duffin, R., Poland, C.A., Howie, S.E., MacNee, W., Bradley, M., Megson, I.L., Donaldson, K., 2010. Metal oxide nanoparticles induce unique inflammatory footprints in the lung: important implications for nanoparticle testing. Environ. Health Perspect. 118 (12), 1699–1706.
Clemens, D.L., Lee, B., Xue, M., Thomas, C.R., Meng, H., Ferris, D., Nel, A.E., Zink, J.I., Horwitz, M.A., 2012. Targeted intracellular delivery of antituberculosis drugs to *Mycobacterium tuberculosis*-infected macrophages *via* functionalized mesoporous silica nanoparticles. Antimicrob. Agents Chemother. 56 (5), 2535–2545.
Costa, P.M., Fadeel, B., 2016. Emerging systems biology approaches in nanotoxicology: towards a mechanism-based understanding of nanomaterial hazard and risk. Toxicol. Appl. Pharmacol. 299, 101–111.
Costa, P.M., Gosens, I., Williams, A., Farcal, L., Pantano, D., Brown, D.M., Stone, V., Cassee, F.R., Halappanavar, S., Fadeel, B., 2018. Transcriptional profiling reveals gene expression changes associated with inflammation and cell proliferation following short-term inhalation exposure to copper oxide nanoparticles. J. Appl. Toxicol. 38 (3), 385–397.
Cui, X., Hwang, J.T.G., Qiu, J., Blades, N.J., Churchill, G.A., 2005. Improved statistical tests for differential gene expression by shrinking variance components estimates. Biostatistics 6 (1), 59–75.
Eslamian, M., Ashgriz, N., 2007. Effect of atomization method on the morphology of spray-generated particles. ASME J. Eng. Mater. Technol. 129 (1), 130–142.
Frei, B., England, L., Ames, B.N., 1989. Ascorbate is an outstanding antioxidant in human blood plasma. Proc. Natl. Acad. Sci. U. S. A. 86 (16), 6377–6381.
Gale, R.J., Winkler, C.A., 1977. Thermal rearrangement of the copper(II)—L-cystine complex. Inorg. Chim. Acta 21, 151–156.
Gardini, D., Blosi, M., Ortelli, S., Delpivo, C., Bussolati, O., Bianchi, M.G., Allegri, M., Bergamaschi, E., Costa, A.L., 2018. Nanosilver: an innovative paradigm to promote its safe and active use. NanoImpact 11, 128–135.
Garnier, A., Tosi, L., 1975. Cu(II)–poly(L-arginine) complexes; potentiometric and spectral characterization of amine and peptide nitrogen ligands. Biopolymers 14 (11), 2247–2262.
Gosens, I., Mathijssen, L.E., Bokkers, B.G., Muijser, H., Cassee, F.R., 2014. Comparative hazard identification of nano- and micro-sized cerium oxide particles based on 28-day inhalation studies in rats. Nanotoxicology 8 (6), 643–653.
Gosens, I., Kermanizadeh, A., Jacobsen, N.R., Lenz, A.G., Bokkers, B., de Jong, W.H., Krystek, P., Tran, L., Stone, V., Wallin, H., Stoeger, T., Cassee, F.R., 2015. Comparative hazard identification by a single dose lung exposure of zinc oxide and silver nanomaterials in mice. PLoS One 10 (5), e0126934.
Gosens, I., Cassee, F.R., Zanella, M., Manodori, L., Brunelli, A., Costa, A.L., Bokkers, B.G., de Jong, W.H., Brown, D., Hristozov, D., Stone, V., 2016. Organ burden and pulmonary toxicity of nano-sized copper (II) oxide particles after short-term inhalation exposure. Nanotoxicology 10 (8), 1084–1095.
Grassian, V.H., O'Shaughnessy, P.T., Adamcakova-Dodd, A., Pettibone, J.M., Thorne, P. S., 2007. Inhalation exposure study of titanium dioxide nanoparticles with a primary particle size of 2 to 5 nm. Environ. Health Perspect. 115 (3), 397–402.
Halappanavar, S., Saber, A.T., Decan, N., Jensen, K.A., Wu, D., Jacobsen, N.R., Guo, C., Rogowski, J., Koponen, I.K., Levin, M., Madsen, A.M., Atluri, R., Snitka, V., Birkedal, R.K., Rickerby, D., Williams, A., Wallin, H., Yauk, C.L., Vogel, U., 2015. Transcriptional profiling identifies physicochemical properties of nanomaterials that are determinants of the *in vivo* pulmonary response. Environ. Mol. Mutagen. 56 (2), 245–264.
Hanagata, N., Zhuang, F., Connolly, S., Li, J., Ogawa, N., Xu, M., 2011. Molecular responses of human lung epithelial cells to the toxicity of copper oxide nanoparticles inferred from whole genome expression analysis. ACS Nano 5 (12), 9326–9338.
Ihaka, R., Gentleman, R., 1996. R: a language for data analysis and graphics. J. Comput. Graph. Stat. 5 (3), 299–314.
Ilves, M., Kinaret, P.A.S., Ndika, J., Karisola, P., Marwah, V., Fortino, V., Fedutik, Y., Correia, M., Ehrlich, N., Loeschner, K., Besinis, A., Vassallo, J., Handy, R.D., Wolff, H., Savolainen, K., Greco, D., Alenius, H., 2019. Surface PEGylation suppresses pulmonary effects of CuO in allergen-induced lung inflammation. Part Fibre Toxicol 16 (1), 28.

Kaplan, J., 2002. Mechanisms of cellular iron acquisition: another iron in the fire. Cell 111 (5), 603–606.
Karlsson, H.L., Cronholm, P., Gustafsson, J., Möller, L., 2008. Copper oxide nanoparticles are highly toxic: a comparison between metal oxide nanoparticles and carbon nanotubes. Chem. Res. Toxicol. 21 (9), 1726–1732.
Kodali, V., Littke, M.H., Tilton, S.C., Teeguarden, J.G., Shi, L., Frevert, C.W., Wang, W., Pounds, J.G., Thrall, B.D., 2013. Dysregulation of macrophage activation profiles by engineered nanoparticles. ACS Nano 7 (8), 6997–7010.
Krämer, A., Green, J., Pollard, J., Tugendreich, S., 2014. Causal analysis approaches in ingenuity pathway analysis. Bioinformatics 30 (4), 523–530.
Lanone, S., Rogerieux, F., Geys, J., Dupont, A., Maillot-Marechal, E., Boczkowski, J., Lacroix, G., Hoet, P., 2009. Comparative toxicity of 24 manufactured nanoparticles in human alveolar epithelial and macrophage cell lines. Part Fibre Toxicol. 6, 14.
Líbalová, H., Costa, P.M., Olsson, M., Farcal, L., Ortelli, S., Blosi, M., Topinka, J., Costa, A.L., Fadeel, B., 2018. Toxicity of surface-modified copper oxide nanoparticles in a mouse macrophage cell line: interplay of particles, surface coating and particle dissolution. Chemosphere 196, 482–493.
Naatz, H., Lin, S., Li, R., Jiang, W., Ji, Z., Chang, C.H., Köser, J., Thöming, J., Xia, T., Nel, A.E., Mädler, L., Pokhrel, S., 2017. Safe-by-design CuO nanoparticles *via* Fe-doping, Cu-O bond length variation, and biological assessment in cells and zebrafish embryos. ACS Nano 11 (1), 501–515.
Ortelli, S., Costa, A.L., Blosi, M., Brunelli, A., Badetti, E., Bonetto, A., Hristozov, D., Marcomini, A., 2017. Colloidal characterisation of CuO nanoparticles in biological and environmental media. Environ. Sci. Nano. 4, 1264–1272.
Pantano, D., Neubauer, N., Navratilova, J., Scifo, L., Civardi, C., Stone, V., von der Kammer, F., Müller, P., Sobrido, M.S., Angeletti, B., Rose, J., Wohlleben, W., 2018. Transformations of nanoenabled copper formulations govern release, antifungal effectiveness, and sustainability throughout the wood protection lifecycle. Environ. Sci. Technol. 52 (3), 1128–1138.
Prá, D., Franke, S.I., Giulian, R., Yoneama, M.L., Dias, J.F., Erdtmann, B., Henriques, J.A., 2008. Genotoxicity and mutagenicity of iron and copper in mice. Biometals 21 (3), 289–297.
Rossner, P., Vrbova, K., Rossnerova, A., Zavodna, T., Milcova, A., Klema, J., Vecera, Z., Mikuska, P., Coufalik, P., Capka, L., Krumal, K., Docekal, B., Holan, V., Machala, M., Topinka, J., 2020. Gene expression and epigenetic changes in mice following inhalation of copper(II) oxide nanoparticles. Nanomaterials 10 (3), 550.
Sanità, G., Carrese, B., Lamberti, A., 2020. Nanoparticle surface functionalization: how to improve biocompatibility and cellular internalization. Front. Mol. Biosci. 7, 587012.
Saporito-Magriñá, C.M., Musacco-Sebio, R.N., Andrieux, G., Kook, L., Orrego, M.T., Tuttolomondo, M.V., Desimone, M.F., Boerries, M., Borner, C., Repetto, M.G., 2018. Copper-induced cell death and the protective role of glutathione: the implication of impaired protein folding rather than oxidative stress. Metallomics 10 (12), 1743–1754.
Shi, M., Kwon, H.S., Peng, Z., Elder, A., Yang, H., 2012. Effects of surface chemistry on the generation of reactive oxygen species by copper nanoparticles. ACS Nano 6 (3), 2157–2164.
Slob, W., 1999. Thresholds in toxicology and risk assessment. Int. J. Toxicol. 18, 259–268.
Slob, W., 2002. Dose-response modeling of continuous endpoints. Toxicol. Sci. 66 (2), 298–312.
Slob, W., Bakker, M.I., Biesebeek, J.D., Bokkers, B.G., 2014. Exploring the uncertainties in cancer risk assessment using the integrated probabilistic risk assessment (IPRA) approach. Risk Anal. 34 (8), 1401–1422.
Strauch, B.M., Niemand, R.K., Winkelbeiner, N.L., Hartwig, A., 2017. Comparison between micro- and nanosized copper oxide and water soluble copper chloride: interrelationship between intracellular copper concentrations, oxidative stress and DNA damage response in human lung cells. Part Fibre Toxicol. 14 (1), 28.
Sun, B., Pokhrel, S., Dunphy, D.R., Zhang, H., Ji, Z., Wang, X., Wang, M., Liao, Y.P., Chang, C.H., Dong, J., Li, R., Mädler, L., Brinker, C.J., Nel, A.E., Xia, T., 2015. Reduction of acute inflammatory effects of fumed silica nanoparticles in the lung by adjusting silanol display through calcination and metal doping. ACS Nano 9 (9), 9357–9372.
Tarasova, N.K., Gallud, A., Ytterberg, A.J., Chernobrovkin, A., Aranzaes, J.R., Astruc, D., Antipov, A., Fedutik, Y., Fadeel, B., Zubarev, R.A., 2017. Cytotoxic and proinflammatory effects of metal-based nanoparticles on THP-1 monocytes characterized by combined proteomics approaches. J. Proteome Res. 16 (2), 689–697.
Toyonaga, T., Matsuura, M., Mori, K., Honzawa, Y., Minami, N., Yamada, S., Kobayashi, T., Hibi, T., Nakase, H., 2016. Lipocalin 2 prevents intestinal inflammation by enhancing phagocytic bacterial clearance in macrophages. Sci. Rep. 6, 35014.
Tuomela, S., Autio, R., Buerki-Thurnherr, T., Arslan, O., Kunzmann, A., Andersson-Willman, B., Wick, P., Mathur, S., Scheynius, A., Krug, H.F., Fadeel, B., Lahesmaa, R., 2013. Gene expression profiling of immune-competent human cells exposed to engineered zinc oxide or titanium dioxide nanoparticles. PLoS One 8 (7), e68415.
Wallin, H., Kyjovska, Z.O., Poulsen, S.S., Jacobsen, N.R., Saber, A.R., Bengtson, S., Jackson, P., Vogel, U., 2017. Surface modification does not influence the genotoxic and inflammatory effects of TiO_2 nanoparticles after pulmonary exposure by instillation in mice. Mutagenesis 32 (1), 47–57.
Wang, Z., Li, N., Zhao, J., White, J.C., Qu, P., Xing, B., 2012. CuO nanoparticle interaction with human epithelial cells: cellular uptake, location, export, and genotoxicity. Chem. Res. Toxicol. 25 (7), 1512–1521.
Wongrakpanich, A., Mudunkotuwa, I.A., Geary, S.M., Morris, A.S., Mapuskar, K.A., Spitz, D.R., Grassian, V.H., Salem, A.K., 2016. Size-dependent cytotoxicity of copper oxide nanoparticles in lung epithelial cells. Environ. Sci. Nano 3 (2), 365–374.
Yan, L., Zhao, F., Wang, J., Zu, Y., Gu, Z., Zhao, Y., 2019. A safe-by-design strategy towards safer nanomaterials in nanomedicines. Adv. Mat. 31 (1805391), 1–33.
Zhang, J., Zou, Z., Wang, B., Xu, G., Wu, Q., Zhang, Y., Yuan, Z., Yang, X., Yu, C., 2018. Lysosomal deposition of copper oxide nanoparticles triggers HUVEC cells death. Biomaterials 161, 228–239.
Zhao, F., Zhao, Y., Liu, Y., Chang, X., Chen, C., Zhao, Y., 2011. Cellular uptake, intracellular trafficking, and cytotoxicity of nanomaterials. Small 7 (10), 1322–1337.